AIAA JOURNAL
Vol. 37, No. 10, October 1999

Effects of Dynamic Stall on Propulsive Efficiency and Thrust of Flapping Airfoil

K. Isogai* and Y. Shinmoto†
Kyushu University, Fukuoka 812-8581, Japan
and
Y. Watanabe‡
Mitsubishi Heavy Industries, Ltd., Nagasaki 850-0063, Japan

Numerical simulations of dynamic stall phenomena around an airfoil oscillating in a coupled mode, in which the pitching and heaving oscillations have some phase difference, have been performed with a Navier–Stokes code. The propulsive efficiency and the thrust have been calculated for various combinations of the phase difference and the reduced frequency for two different amplitude ratios. The effects of the dynamic stall phenomena on the behaviors of the propulsive efficiency and thrust are discussed in detail by examination of each flow pattern obtained. Highest efficiency has been observed for the case in which the pitching oscillation advances 90 deg ahead of the heaving oscillation and the reduced frequency is at some optimum value, for which there appears no appreciable flow separation in spite of large-amplitude oscillations. For phase angles and reduced frequency other than this best condition, efficiency is rapidly degraded by the occurrence of the large-scale leading-edge separation.

Nomenclature

a	= dimensionless axis of pitch
b	= semichord length
C	= chord length
C_p	= pressure coefficient $[(p - p_\infty)/(1/2\rho U^2)]$
C_T	= thrust coefficient [Eq. (9)]
c	= propagation velocity of wave
$f(x, t)$	= dimensionless displacement of airfoil
h	= dimensionless displacement of heaving oscillation
h_0	= dimensionless amplitude of heaving oscillation
k	= reduced frequency $(b\omega/U)$
M	= freestream Mach number
p	= pressure
Re	= Reynolds number (UC/ν)
T	= time
$\bar{T}$	= mean thrust
t	= dimensionless time $[T(U/b)]$
U	= freestream velocity
$\bar{W}$	= mean work rate
x, y	= Cartesian coordinates, nondimensionalized by semichord
α	= angular displacement
α_0	= amplitude of pitching oscillation
ζ	= dimensionless vorticity $[\zeta = (\partial v/\partial x - \partial u/\partial y)/2]$
η_p	= propulsive efficiency [Eq. (8)]
ν	= kinematic viscosity
ρ	= air density
τ	= kt (reduced frequency × dimensionless time)
ϕ	= phase advance angle of pitching oscillation ahead of heaving oscillation
ω	= circular frequency

Subscript

∞	= freestream quantity

Presented as Paper 97-1926 at the AIAA 28th Fluid Dynamics Conference, Snowmass Village, CO, 29 June–2 July 1997; received 5 August 1997; revision received 2 January 1999; accepted for publication 15 March 1999.

*Professor, Department of Aeronautics and Astronautics. Associate Fellow AIAA.
†Research Assistant, Department of Aeronautics and Astronautics.
‡Deputy Chief Researcher, Nagasaki Research and Development Center.

Introduction

MANY experimental and theoretical studies have been conducted[1] on the generation of propulsive force by the flapping motions of a wing. If we confine our attention to a two-dimensional flapping airfoil, the following works are notable. The classical works of Garrick,[2] Lighthill,[3] and Wu[4] are all based on flat-plate potential-flow theory. Later, Faigrieve and Delaurier[5] developed a flat-plate potential-flow theory, which can treat large-amplitude oscillations. Platzer et al.[6] and Jones and Platzer[7] developed a panel method that can take into account the airfoil thickness effects. Although these potential theories have contributed considerably to the understanding of the mechanism of thrust generation of a flapping airfoil, the results obtained do not necessarily explain many features, especially when the amplitudes of the pitching and heaving oscillations are large, which is the common feature of bird flight. For example, the effective angle of attack of the flapping airfoil easily reaches to the static-stalling angle and even goes beyond that angle to several tens of degrees, depending on the reduced frequency. Therefore it is indispensable to take into account the effects of dynamic stall phenomena for estimating propulsive efficiency and thrust of a flapping airfoil. The importance of such analysis is also pointed out by Delaurier[8] and Fairgrieve and Delaurier.[5] Recently Tuncer and Platzer[9] conducted a numerical study on the viscous and nonlinear effects on the thrust and propulsive efficiency of an airfoil oscillating in pure plunging mode by using a Navier–Stokes code. They obtained the results that, at low reduced frequency and amplitude flapping motions, the viscous and the nonlinear effects dominate the average thrust and reduce the propulsive efficiency significantly. As is well known, however, the flapping motion of bird flight is a coupled pitching and heaving oscillation with some phase difference between them. Therefore it is quite interesting to see the viscous effects (especially the effects of dynamic stall phenomena) on thrust and propulsive efficiency for various combinations of the reduced frequency, the phase difference between the pitching and heaving oscillations, and the amplitude ratio between them.

The purpose of this paper is to clarify the effects of dynamic stall phenomena on the propulsive efficiency and the thrust of an airfoil oscillating in a coupled pitching and heaving mode for various combinations of reduced frequency, phase difference, and amplitude ratio between them. For this purpose, the numerical simulation technique of using a Navier–Stokes code is used.

Numerical Method and Code Validation

The computer code[10] used for the present study, which has been developed by one of the present authors, is based on the compressible

Navier–Stokes equations. The finite difference scheme used is the Yee–Harten total variation diminishing (TVD) scheme.[11] In most of the calculations, Re is assumed to be of the order of 10^5 and a Baldwin and Lomax[12] algebraic turbulence model is used. Several computations in which laminar flow is assumed are also performed for comparison with the turbulence case. The C-type grid of 280×80 (200 points on the airfoil) points is used, and a freestream boundary condition is prescribed at the far-field boundary, which is located $\mathcal{O}10$ chords away from the airfoil. The no-slip boundary condition is given on the airfoil surface. The law of the wall coordinate y_{+1} of the grid points next to the airfoil surface is $\mathcal{O}1.0$. All computations are performed at $M = 0.30$. The periodic solutions are usually obtained after two to four cycles of oscillation. The convergence is confirmed by the fact that the differences of propulsive efficiencies and thrust coefficients obtained for the final two cycles of oscillation are less than 1%.

The capability of the present code for calculating unsteady viscous flows around an oscillating airfoil is extensively examined in Ref. 10. Another example, which demonstrates the capability of the present code for calculating dynamic stall phenomena, is shown in Fig. 1. In Fig. 1, the behavior of the dynamic stall vortex on the NACA0012 airfoil oscillating in pitch, which is simulated by the present code, is compared with the schlieren pictures obtained by Chandrasekhara and Carr[13] in their flow visualization study. The airfoil is oscillated in pitch about the quarter-chord axis at a mean angle of attack of 10 deg with an amplitude of ±10 deg. M is 0.30, Re is 1.0×10^5, and k is 0.10. The Baldwin and Lomax algebraic turbulence model[12] is used in the computation. As seen from Fig. 1 (isodensity contours are plotted for the computed results), the dynamic stall vortex observed in the experiment is well captured by the present code in the qualitative sense. However, some quantitative discrepancy can be seen in the propagation velocity of the dynamic stall vortex, that is, the propagation velocity of the dynamic stall vortex in the experiment is approximately 30% of the freestream velocity, and that obtained by the present computation is approximately 20% of the freestream velocity. The reason for this discrepancy is not known, but it might be attributed to the inadequacy of the Baldwin and Lomax model. Further investigation on this point is needed. Although some quantitative discrepancy is observed between the computation and the experiment, it seems still to be of some importance to investigate qualitatively the effects of the dynamic stall phenomena on the thrust generation of a flapping airfoil. For this purpose the present code seems to have enough capability. The reliability of the present code for calculating the thrust and propulsive efficiency is examined in the following sections by comparison of the present results with other existing results, namely, Lighthill's flat-plate potential-flow theory[3] and the Navier–Stokes computations by Tuncer et al.[14] and Tuncer and Platzer.[15]

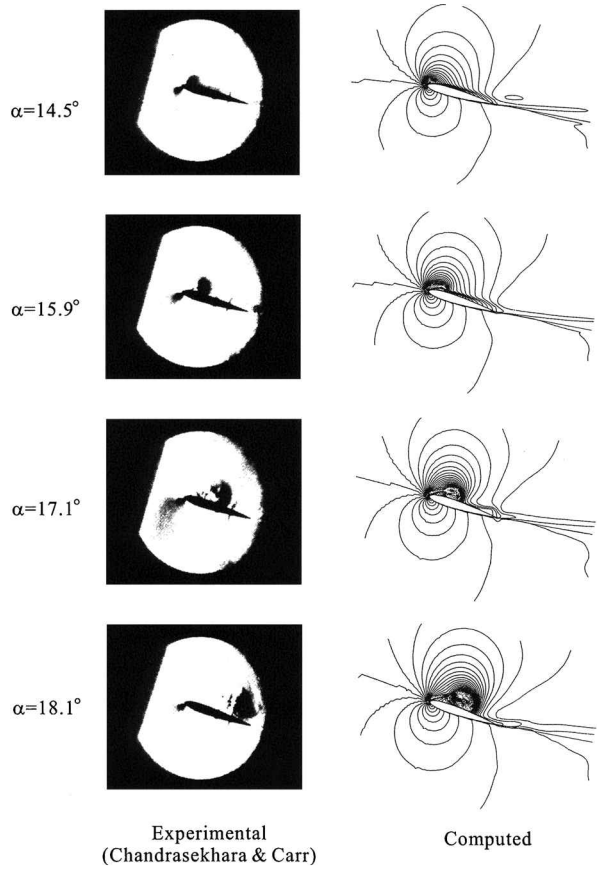

Fig. 1 Comparison of computed and experimental flow patterns around NACA0012 airfoil oscillating in pitch ($M = 0.30$, $Re = 1.0 \times 10^5$, $k = 0.10$, $\alpha = 10$ deg + 10 deg sin kt).

Definition of Airfoil Motion

In Fig. 2, the airfoil motion is defined, where h is the displacement of the pitch axis located at $x = a$ and α is the angular displacement. All of the physical quantities are nondimensionalized by the semichord b and the freestream velocity U. The airfoil section used in the present study is NACA0012. In the present study, the mean angle of attack is assumed to be zero, that is, the mean lift and pitching moments are zero. The focus is on the computations of only mean thrust and propulsive efficiency. Therefore h and α can be expressed as

$$h = h_0 \sin kt \tag{1}$$

$$\alpha = \alpha_0 \sin(kt + \phi) \tag{2}$$

From Eqs. (1) and (2), the displacement of an arbitrary point x of the mean surface of the airfoil in the y direction at time t can be expressed as

$$f(x, t) = \sqrt{A^2 + B^2}\sin(kt - \psi) \tag{3}$$

where

$$A = h_0 - (x - a)\alpha_0 \cos\phi, \qquad B = (x - a)\alpha_0 \sin\phi$$
$$\psi = \tan^{-1}(B/A) \tag{4}$$

Equation (3) can be expressed approximately as

$$f(x, t) = \sqrt{A^2 + B^2}\sin\left[kt - \left(\overline{\frac{d\psi}{dx}}\right)x\right] \tag{5}$$

where $(\overline{d\psi/dx})$ is the mean value of $(d\psi/dx)$ over the airfoil chord. It can be identified from Eq. (5) that the coupled motion expressed by Eq. (3) produces wave motion propagating in the x direction. It is clear that the origin of this wave motion can be attributed to the coupled heaving and pitching oscillations with a finite phase difference. When we define the propagation velocity of the wave as c, c/U can be given by

$$\frac{c}{U} = k \Big/ \left(\overline{\frac{d\psi}{dx}}\right) \tag{6}$$

from Eq. (5).

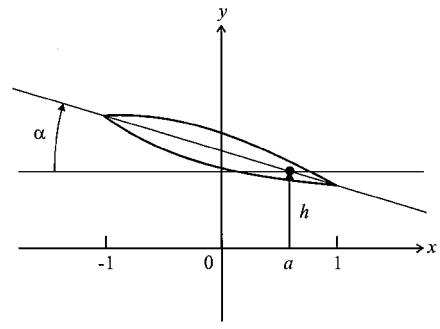

Fig. 2 Definition of airfoil motion.

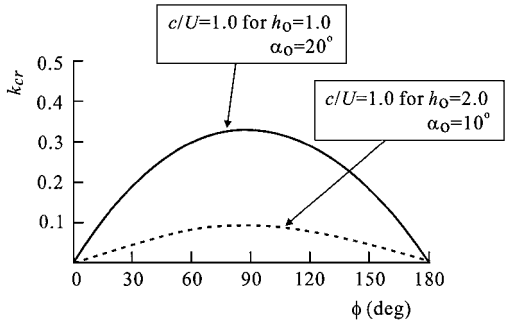

Fig. 3 Behavior of k_{cr}.

Bschorr[16] has pointed out, from the discussion based on the quasi-steady inviscid flow assumptions, that if $c/U > 1$ then propulsive force or thrust is produced and if $c/U < 1$ then flutter may occur or drag force is produced. When we denote k_{cr} as the critical reduced frequency, which gives $c/U = 1$, k_{cr} is given by

$$k_{cr} = \left(\overline{\frac{d\psi}{dx}}\right) \tag{7}$$

which is a function of a, α_0/h_0, and ϕ.

This argument, which is based on the inviscid and quasi-steady flow assumptions, must be modified by the unsteady and dynamic stall effects. However, the behavior of k_{cr} given by Eq. (7) is still useful to select the parameters such as k, ϕ, h_0, and α_0 for which the numerical simulations are to be performed. For this reason, the behavior of k_{cr} on the $k-\phi$ plane is plotted in Fig. 3 for the two different amplitude ratios, namely,

case A, $h_0 = 1.0$, $\alpha_0 = 20\,\text{deg}$, $a = 0$

case B, $h_0 = 2.0$, $\alpha_0 = 10\,\text{deg}$, $a = 0$

As seen from Fig. 3, k_{cr} depends strongly on the amplitude ratio and phase difference. The present numerical simulations have been performed for various combinations of k and ϕ for each of these two cases.

Before we present the results of the numerical simulations, the definitions of propulsive efficiency η_p and the thrust coefficient C_T need to be given.[3] The propulsive efficiency η_p is defined by

$$\eta_p = (\bar{T}U)/\bar{W} \tag{8}$$

where $\bar{T}$ is the mean thrust during one cycle of airfoil oscillation and $\bar{W}$ is the mean rate at which the airfoil motion does work against the surrounding fluid during one cycle of oscillation. The thrust coefficient C_T is defined as

$$C_T = \frac{\bar{T}}{\left(\frac{1}{2}\right)\rho U^2 (kh_0)^2 (2b)} \tag{9}$$

$\bar{T}$ in Eqs. (8) and (9) can be given by

$$\bar{T} = -\frac{1}{2\pi}\int_0^{2\pi}\left[\left(\frac{1}{2}\right)\rho U^2 b \oint C_p\left(\frac{dy}{dx} + f_x\right)x_\xi \, d\xi\right] d\tau \tag{10}$$

where $y = y(x)$ gives the airfoil contour, f_x is the x derivative of f given by Eq. (3), ξ is the independent variable taken along the airfoil contour in the computational domain,[10] and $\oint$ means the integral around the airfoil contour. As seen from Eq. (10), the friction drag is not taken into account in the present study.

$\bar{W}$ in Eq. (8) can be calculated by

$$\bar{W} = \frac{U}{2\pi}\int_0^{2\pi}\left[\left(\frac{1}{2}\right)\rho U^2 b \oint C_p f_t x_\xi \, d\xi\right] d\tau \tag{11}$$

where f_t is the t derivative of f given by Eq. (3).

Results and Discussion

As mentioned in the preceding section, the present numerical simulations have been performed for various combinations of k and ϕ for each of the two different amplitude ratios α_0/h_0, that is, case A ($h_0 = 1.0$, $\alpha_0 = 20$ deg, $a = 0$) and case B ($h_0 = 2.0$, $\alpha = 10$ deg, $a = 0$).

a) Case A ($h_0 = 1.0$, $\alpha_0 = 20$ deg, $a = 0$). In Fig. 4, the points on the k–ϕ plane for which the numerical simulations have been done are indicated by the symbols ○, ◌́, ●, and ◌́, together with the behavior of k_{cr} discussed in the preceding section. The symbols ○ and ◌́ denote when thrust is computed, whereas the symbols ● and ◌́ denote when the drag force is computed. The tailed symbols ◌́ and ◌́ mean that the large-scale leading-edge separation vortex is observed in the flow pattern. The number shown in the parentheses just under the symbols ○ and ◌́ is the propulsive efficiency obtained.

As seen from Fig. 4, the highest efficiency of $\eta_p = 0.72$ is obtained for $\phi = 90$ deg and $k = 0.50$, for which the flow pattern (isovorticity contour ζ) is shown in Fig. 5. As seen in Fig. 5, no appreciable flow separation is observed for this case. (We have examined the instantaneous isovorticity contour plot at every phase of the oscillation cycle, observing no indication of appreciable flow separation.)

When the combination of k and ϕ deviates from this best condition, however, the propulsive efficiency decreases rapidly, as seen in Fig. 4. It is obvious that the occurrence of the dynamic stall phenomena is partly responsible for this, as evidenced by Fig. 4. In fact, at many points in the k–ϕ plane, the large-scale leading-edge separation vortex is observed in the flow pattern. For example, the typical flow patterns obtained at $k = 0.50$ and 1.0 for $\phi = 30$ deg are shown in Fig. 6, where $\eta_p = 0.01$ for $k = 0.50$ and the drag force is obtained for $k = 1.0$.

The typical flow patterns obtained for $\phi = 60$ deg at $k = 0.50$ and 1.0 are shown in Figs. 7a and 7b, respectively. In this case, no large-scale separation is observed for $k = 0.50$, but the large-scale leading-edge separation vortex is observed for $k = 1.0$. It should be noted, however, that for $k = 1.0$ thrust is still produced in spite of the large-scale separation [although the propulsive efficiency ($\eta_p = 0.27$) is not so high].

Why is the behavior of the dynamic stall phenomena so dependent on the combinations of k and ϕ? To understand this, it is quite useful

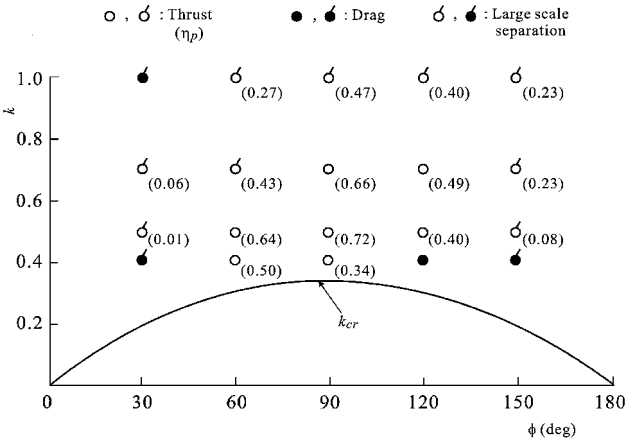

Fig. 4 Results of numerical simulation (case A; $h_0 = 1.0$, $\alpha = 20$ deg, $a = 0$).

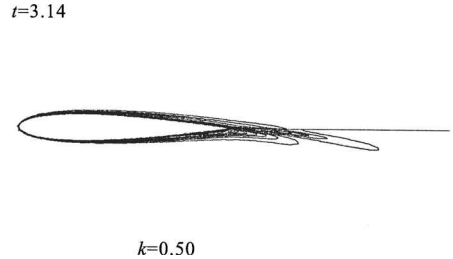

Fig. 5 Isovorticity contour ($\phi = 90$ deg).

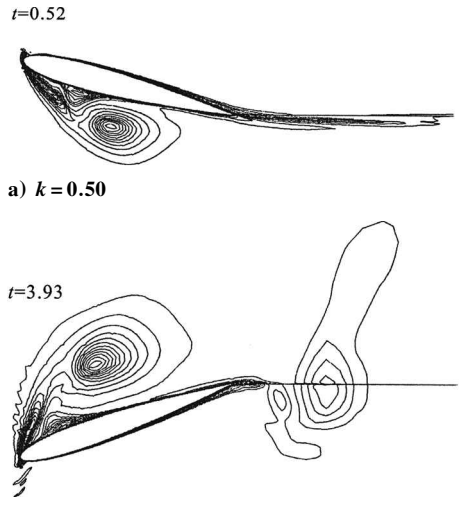

a) $k = 0.50$

b) $k = 1.0$

Fig. 6 Isovorticity contour ($\phi = 30$ deg).

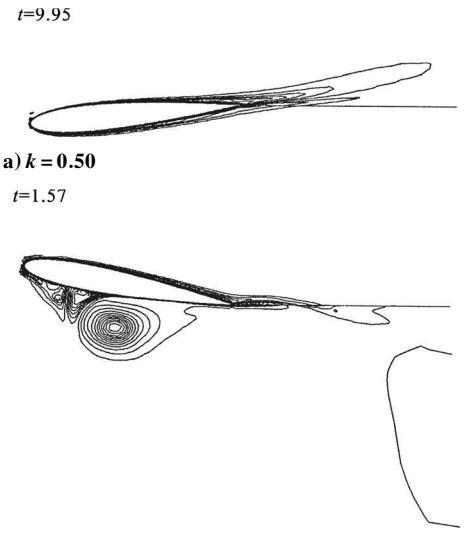

a) $k = 0.50$

b) $k = 1.0$

Fig. 7 Isovorticity contour ($\phi = 60$ deg).

to examine the behavior of the effective angle of attack induced by the coupled pitching and heaving oscillations. With the assumption of a quasi-steady flow, the effective angle of attack induced by the coupled pitching and heaving oscillations is given by

$$\alpha_e = \tan^{-1}\left(-\frac{\mathrm{d}h}{\mathrm{d}t}\right) + \alpha \tag{12}$$

Substituting Eqs. (1) and (2) into Eq. (12), we obtain

$$\alpha_e = \tan^{-1}(-kh_0 \cos kt) + \alpha_0 \sin(kt + \phi) \tag{13}$$

It is easy to calculate the maximum value of α_e, namely $|\alpha_e|_{\max}$, from Eq. (13). In Fig. 8, the behavior of $|\alpha_e|_{\max}$ is plotted against k with ϕ as a parameter. The points for which the present numerical simulations are performed are also plotted by the symbols ○, ◌, ●, and ◐, whose meanings are the same as those of Fig. 4. In addition to this, the curve indicating the condition of $c/U = 1.0$ is also shown by the dotted curve. As seen from Fig. 8, the effective angle of attack for $\phi = 90$ deg always gives the lowest values compared with the other values of ϕ throughout the range of the reduced frequency. On the other hand, the effective angle of attack for $\phi = 30$ and 150 deg reaches relatively high values of 20–40 deg for $k = 0.40$–1.0, experiencing a large-scale leading-edge separation.

In Fig. 9, the behavior of the propulsive efficiency η_p with respect to ϕ is plotted with k as a parameter. The efficiency is rapidly

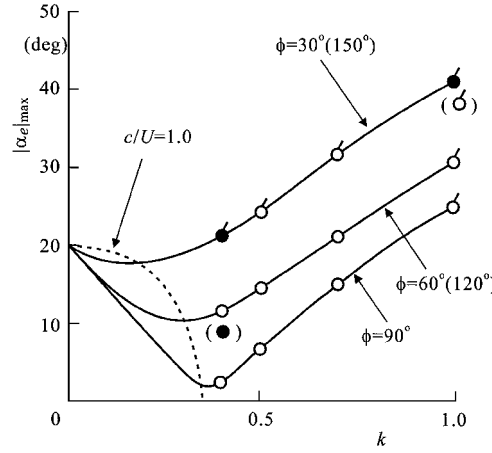

Fig. 8 Behavior of effective angle of attack (case A).

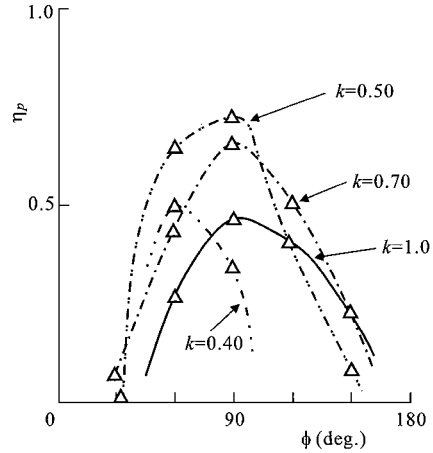

Fig. 9 Propulsive efficiency (case A).

degraded as ϕ differs from 90 deg. It is clear that the dynamic stall phenomenon is responsible for the considerable part of these trends of η_p.

In Fig. 10, the thrust coefficient C_T is plotted with respect to the phase angle ϕ. For $k = 1.0$ the maximum value of C_T is obtained near $\phi = 120$ deg rather than 90 deg.

In Figs. 11 and 12, the behaviors of η_p and C_T, respectively, with respect to k for $\phi = 90$ deg are plotted and compared with those predicted by Lighthill's flat-plate potential theory.[3] The results obtained by assuming an inviscid flow (Euler code results) and those obtained by assuming a laminar flow are also plotted, respectively, for comparison with those obtained with the turbulence model. The differences between the inviscid flow results and those of the flat-plate potential theory might be attributed to the effects of the airfoil thickness and the finite amplitude of the oscillation. It can be seen that viscous effects reduce both the propulsive efficiency and the thrust coefficient. It is also interesting to see that the almost identical values of η_p and C_T are predicted whether we assume laminar flow or turbulent flow for this particular case. This is quite different from the phenomena observed in the usual steady or quasisteady flows. It is conjectured that, as concerns propulsive efficiency and thrust coefficients, the difference between laminar flow and turbulent flow becomes small at those high reduced frequencies. It should be noted that no appreciable flow separation has been observed for $k = 0.50$ and 0.70 for both laminar and turbulent flows. For $k = 1.0$, the dynamic stall vortices appear for both the laminar and the turbulent cases, as shown in Fig. 13. However, the flow patterns for both cases are quite similar to each other, although there seems to be some small difference in the detailed flow structures within the vortex. These observations might explain the results, although further investigation is needed to clarify this phenomenon.

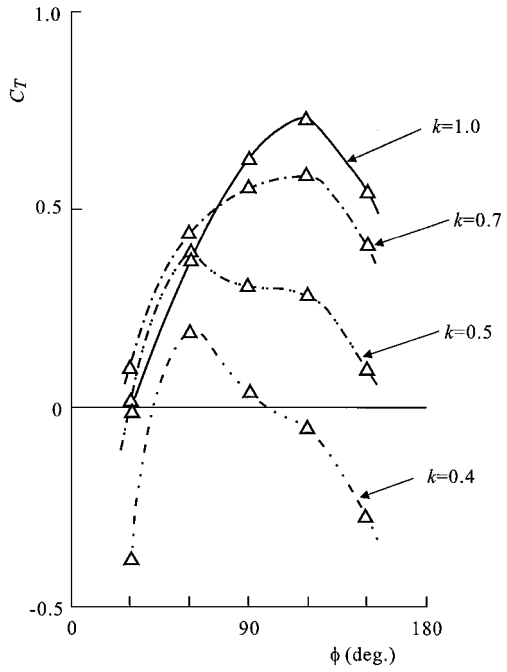

Fig. 10 Thrust coefficient (case A).

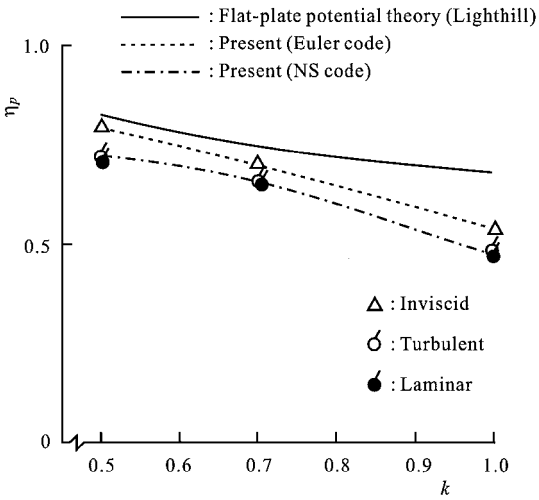

Fig. 11 Comparison of propulsive efficiency with flat-plate potential theory: NS, Navier–Stokes.

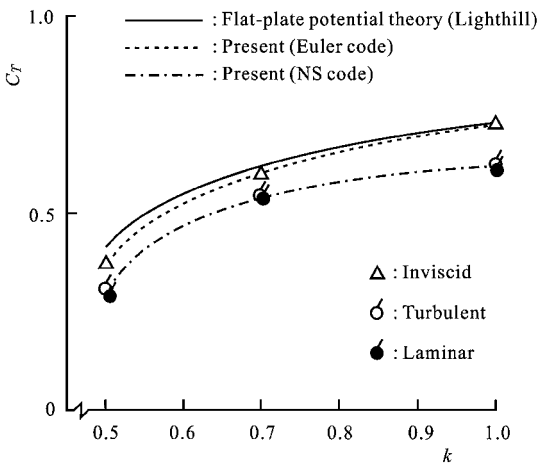

Fig. 12 Comparison of thrust coefficient with flat-plate potential theory.

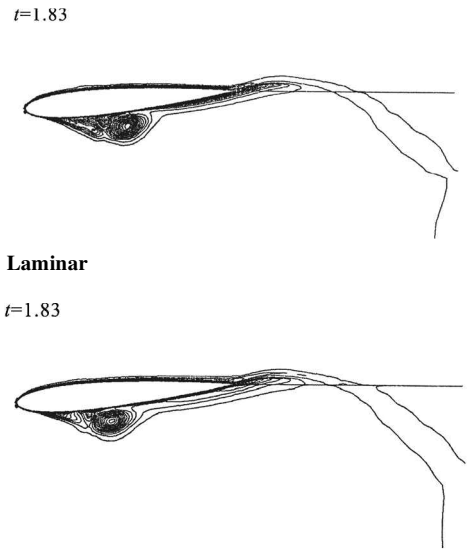

Fig. 13 Isovorticity contour ($\phi = 90$ deg, $k = 1.0$).

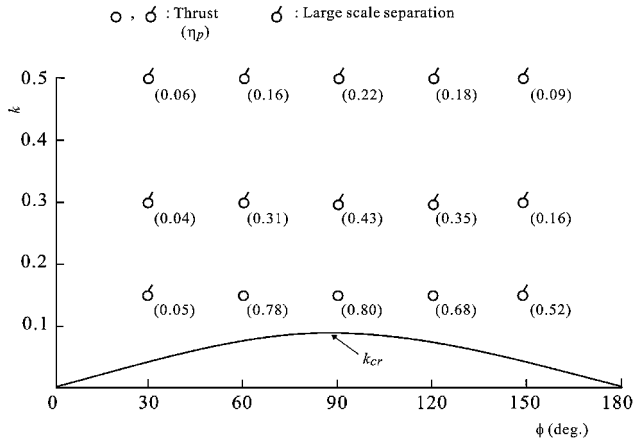

Fig. 14 Results of numerical simulation (case B; $h_0 = 2.0$, $\alpha = 10$ deg, $a = 0$).

b) Case B ($h_0 = 2.0$, $\alpha_0 = 10$ deg, $a = 0$). In Fig. 14, the points on the k–ϕ plane for which the numerical simulations have been done are shown by the symbols ○ and ◌́. The behavior of k_{cr} as discussed in the preceding section is also plotted. The meanings of each symbol are the same as those of case A. The highest efficiency ($\eta_p = 0.80$) is obtained for $\phi = 90$ deg and $k = 0.15$. Again, efficiency is rapidly degraded as k increases and ϕ differs from 90 deg. The typical flow patterns obtained at $k = 0.15$, 0.30, and 0.50 for $\phi = 90$ deg are shown in Figs. 15a, 15b, and 15c, respectively. No large-scale separation is observed for $k = 0.15$, but the large-scale leading-edge separation vortex is observed for $k = 0.30$ and 0.50. This is attributed to the large effective angle of attack (approximately 20–35 deg) induced by the large-amplitude heaving oscillation at large values of k. This can be seen in Fig. 16, in which the behaviors of the effective angle of attack $|\alpha_e|_{\max}$ are plotted against k together with the points for which the present numerical simulations have been performed. As seen from the figure, the large-scale leading-edge separation is observed at all the points where $|\alpha_e|_{\max} \geq 15$–20 deg.

In Figs. 17 and 18, η_p and C_T, respectively, are plotted against ϕ with k as a parameter. The results obtained by Tuncer et al.[14] are also plotted for comparison. They also used a Navier–Stokes code with the Baldwin and Lomax turbulence model. Although the agreements between the two computations are fairly good for $\phi \geq 60$ deg, the large quantitative discrepancies are seen in both η_p and C_T for $\phi = 30$ deg. For $\phi = 30$ deg the severe leading-edge flow separations have been observed in our computations for all of the

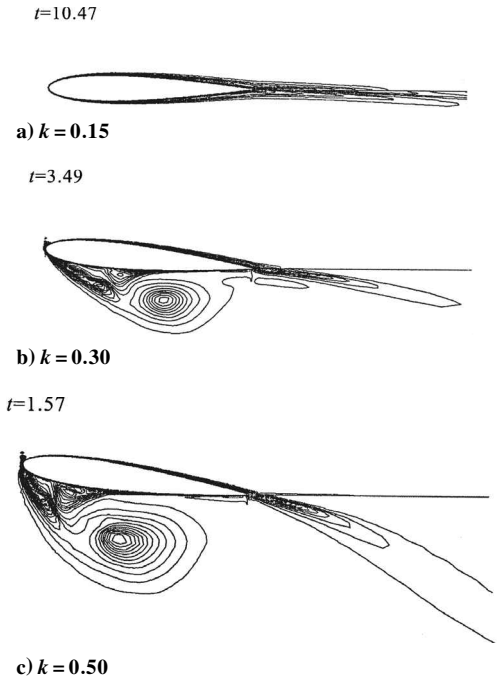

Fig. 15 Isovorticity contour ($\phi = 90$ deg).

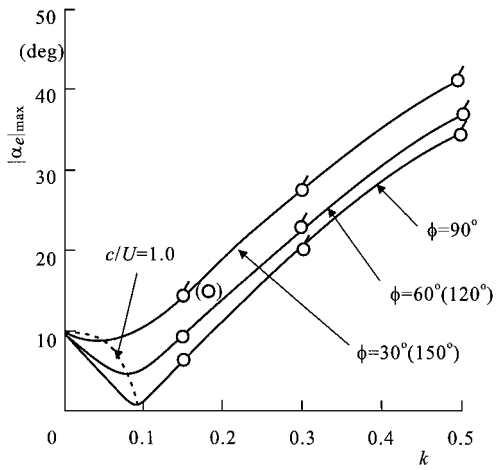

Fig. 16 Behavior of effective angle of attack (case B).

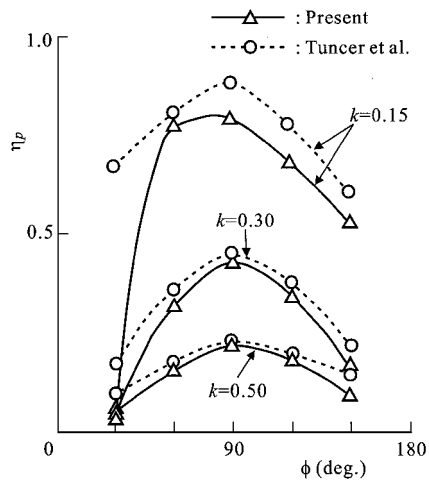

Fig. 17 Propulsive efficiency (case B).

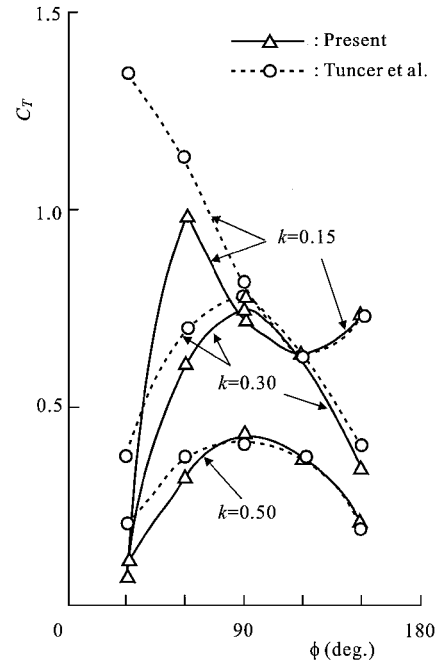

Fig. 18 Thrust coefficient (case B).

reduced frequencies computed, whereas no flow separation has been observed for $k = 0.15$ in the computations by Tuncer and Platzer.[15] However, the reason for these discrepancies is not known and needs further investigation.

It is interesting to see in Fig. 18 that the highest C_T is obtained for $k = 0.15$ and $\phi = 60$ deg. This is a different trend from that of case A, for which the highest C_T is obtained for $k = 1.0$ and $\phi = 120$ deg. It is clear that the low values of C_T and poor efficiency obtained for $k = 0.50$ can be attributed to the occurrence of large-scale leading-edge separation.

Conclusion

Numerical simulations of the dynamic stall phenomena around an airfoil oscillating in a coupled mode, in which the pitching and heaving oscillations have some phase differences, have been performed with a Navier–Stokes code. The propulsive efficiency and thrust have been calculated for various combinations of the phase difference and the reduced frequency for two different amplitude ratios. The effects of the dynamic stall phenomena on the behaviors of the propulsive efficiency and thrust are discussed in detail by examination of each flow pattern obtained. The highest efficiency has been observed for the case in which the pitching oscillation advances 90 deg ahead of the heaving oscillation and the reduced frequency is at some optimum value for which no appreciable flow separation appears, in spite of the large-amplitude oscillations. For phase angles and reduced frequency other than this best condition, efficiency is rapidly degraded by the occurrence of the large-scale leading-edge separation.

References

[1]Azuma, A., *The Biokinetics of Flying and Swimming*, Springer–Verlag, New York, 1992, Chap. 4.

[2]Garrick, I. E., "Propulsion of Flapping and Oscillating Airfoil," NACA Rept. 567, 1936, pp. 419–427.

[3]Lighthill, M. J., "Aquatic Animal Propulsion of High Hydromechanical Efficiency," *Journal of Fluid Mechanics*, Vol. 44, Pt. 2, 1970, pp. 265–301.

[4]Wu, T. Y., "Hydromechanics of Swimming Propulsion, Part 2: Some Optimum Shape Problems," *Journal of Fluid Mechanics*, Vol. 46, Pt. 3, 1971, pp. 521–544.

[5]Faigrieve, J. D., and Delaurier, J. D., "Propulsive Performance of Two-Dimensional Thin Airfoils Undergoing Large-Amplitude Pitch and Plunge Oscillations," Univ. of Toronto, Inst. of Aerospace Studies, UTIAS TN 226, Downsview, ONT, Canada, 1982.

[6]Platzer, M. F., Neace, K. S., and Pang, C. K., "Aerodynamic Analysis of Flapping Wing Propulsion," AIAA Paper 93-0484, Jan. 1993.

[7]Jones, K. D., and Platzer, M. F., "Numerical Computation of Flapping Wing Propulsion and Power Extraction," AIAA Paper 97-0826, Jan. 1997.

[8]Delaurier, J. D., "An Aerodynamic Model for Flapping Wing Flight," *Aeronautical Journal*, Vol. 97, No. 964, 1993, pp. 125–130.

[9]Tuncer, I. H., and Platzer, M. F., "Thrust Generation Due to Airfoil Flapping," *AIAA Journal*, Vol. 34, No. 2, 1996, pp. 324–331.

[10]Isogai, K., "Numerical Simulation of Dynamic Stall of NACA0012 Airfoil near Static Stall Angle Using the Navier–Stokes Equations," National Aerospace Lab., NAL TR-1141T, Tokyo, March 1992.

[11]Yee, H. C., and Harten, A., "Implicit Scheme for Hyperbolic Conservation Laws in Curvilinear Coordinates," AIAA Paper 85-1513, July 1985.

[12]Baldwin, B. S., and Lomax, H., "Thin Layer Approximation and Algebraic Model for Separated Turbulent Flows," AIAA Paper 78-257, Jan. 1978.

[13]Chandrasekhara, M. S., and Carr, L. W., "Flow Visualization Studies of the Mach Number Effects on the Dynamic Stall of Oscillating Airfoil," AIAA Paper 89-0023, Jan. 1989.

[14]Tuncer, I. H., Walz, R., and Platzer, M. F., "A Computational Study on the Dynamic Stall of a Flapping Airfoil," AIAA Paper 98-2519, June 1998.

[15]Tuncer, I. H., and Platzer, M. F., "A Computational Study of Flow Separation Characteristics and Wake Profiles Behind a Flapping Airfoil," AIAA Paper 99-0648, Jan. 1999.

[16]Bschorr, O., "Propulsive Mechanics in Animal Swimming and Flying Locomotion," *Aeronautical Journal*, Vol. 92, No. 912, 1988, pp. 84–90.

P. R. Bandyopadhyay
Associate Editor